

Modeling and Uncertainty Quantification of Motion of Lung Tumors for Image Guided Radiation Therapy

Ravi Kumar Tarunraj Singh Puneet Singla
Graduate Student Professor Assistant Professor
rkumar6@buffalo.edu tsingh@buffalo.edu psingla@buffalo.edu

*Department of Mechanical & Aerospace Engineering
University at Buffalo, Buffalo, NY-14260.*

Abstract—Target localization is a key issue in the image guided radiation therapy procedures for treating tumors in thorax and abdomen. Breathing induced tumor motion necessitates larger margins during radiation therapy planning which may be harmful for healthy tissue surrounding the tumor. Large sampling time in data acquisition and latencies involved in real time imaging systems and tracking system pose a significant challenge to target localization. A framework based on pulmonary mechanics is developed to predict and precisely track the breathing induced motion of lung tumor to direct the tracking system to an estimated position instead of an observed one. A hybrid approach based on the correlation of real-time imagery data of internal markers and easy to measure external respiratory signals like flow readings etc., is proposed to support dynamic radiation therapy procedures. Issues related to reliability of proposed model predictions in the presence of parametric uncertainty are explored using Polynomial Chaos Expansion.

I. INTRODUCTION

Radiation therapy is a medical procedure which utilizes ionizing radiations such as electron, proton and other high energy particles to control the growth of cancerous tumors. Beams of ionizing radiations have to be precisely targeted to the three dimensional shape of the target tumor volume while avoiding the surrounding healthy tissue. When dealing with tumors in thorax and abdominal region this task becomes increasingly difficult due to movement of the target tumor volume through the course of treatment [1]. Motion of tumors in thorax and abdominal region is mainly induced due to quasi-periodic breathing patterns. This movement can be significant for tumors in the thorax region e.g, lung and breast tumors [2]. This constant movement of tumors during the radiation therapy procedure presents a key problem for radiation therapy procedure as the position of the tumor is not exactly known. Uncertainties in localizing the tumor volume during the radiation therapy necessitates incorporating margins to compensate for movement of the tumor. Inclusion of these margins lead

to increased toxicity associated with radiation therapy as normal tissue inside the Planned Target Volume (PTV) also gets damaged. Examples of the side effects have been well documented in many studies, for example in cases of radiation therapy applied to breast cancer patients, the side effects can include ischemic heart disease, pneumonitis and pulmonary fibrosis, erythema, telangiectasia and ulceration of the skin, and bone necrosis in the ribs and sternum [3], [4]. Most of these side effects have been attributed to normal tissue damage resulting from uncertainty in tumor volume localization due to breathing induced motion and set up errors [3], [5]. Radiation oncologists have to carefully weigh the clinical benefits of treatment with the risks posed to long term quality of life of the patient while deciding on the quantity of radiation dosage. This tradeoff due to uncertainty in localizing the tumor volume can also compromise the effectiveness of radiation therapy by preventing effective dose escalation required for good treatment.

Recent advances in radiation therapy procedures, computing hardware and faster image processing algorithms have enabled treatment procedures for moving target volumes using dynamic Image Guided Radiation Therapy (IGRT) [6]. In this approach the tumor(or fiducial markers implanted in its vicinity) is imaged using 2D or 3D scans during the course of radiation therapy and its location in 3D is identified [7], [8]. This scheme is shown in figure 1. Using this information, the radiation beam can be dynamically directed to the identified tumor location. Although this framework seems appropriate for accurate localization of tumor volumes for 4D (on-line) radiation therapy there are some limitations of this approach. The first issue is that X-ray imaging performed during the course of treatment also represents small radiation dosage to a large area surrounding the tumor volume so imaging, X-ray, CT scans, etc., at a high sampling rate becomes prohibitive. This means that

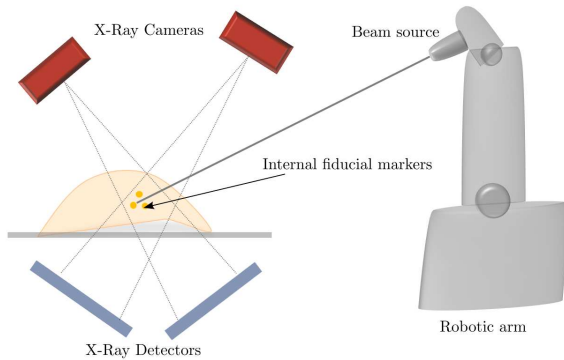


Fig. 1. Image Guided Radiation Therapy

treatment during the time when imaging data is not available has to be guided by some other technique. Secondly, when image is available at particular instant there is a finite time required for the image processing software to analyze and extract the position of the tumor and in the mean time the tumor is still in motion. So the information about the 3D location of tumor volume given by the imaging system is actually not the position at current time. Figure 2 shows the time sequence of imaging and treatment events. Here Δt is the X-ray image sampling time and Δt_1 is the image processing time. Due to this delay in image processing the system has no information about the location of the tumor during the period $\Delta t + \Delta t_1$. Further, the treatment has to be started at time $t + \Delta t_1$ using the position of the tumor at time t , when the image was captured.

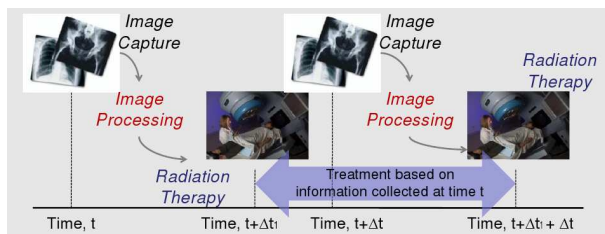


Fig. 2. Treatment delays due to imaging system and system latencies

Another problem with this method is that even when the information from imaging system is available, there are delays associated with control system processing and positioning of the Robotic arm which again means that the tumor location has to be predicted to compensate for these delays.

Current research in dynamic tumor tracking aimed at mitigating these problems is divided into two main categories. The first approach is to come up with prediction algorithms based on time history of past 3D tumor positions [9], [10]. These algorithms predict the future tumor position based on past history of 3D tumor positions. The

second is related to finding the relationship between the tumor motion and external surrogate(external respiration signal) [11], [12]. This is a hybrid approach in which the low sampled information from X-ray imaging is combined with high sampled information from some other respiration signals(also termed as external surrogate) like displacement of external chest markers, strain gauge, pneumo-tachograph etc, [13]. The aim is to find the correlation model or correspondence map between the external surrogate and tumor motion so treatment during the time when imaging information is not available can be carried out on the basis of tumor location inferred from these models.

In this paper, the problem of modeling related to the latter category is addressed i.e, finding a model between a suitable external surrogate and motion of the tumor. For the proposed model we also discuss the issue of uncertainty in the model parameters and develop a framework to find uncertainty measures which can be used for finding optimal image sampling times.

II. TUMOR MOTION MODELING

In this section we present the details of a model for lung tumor motion which is based on the pulmonary mechanics. We also present brief details of other models used for comparing the performance of the proposed method.

A. Prediction Model

Most of the methods for finding the correspondence map between different external surrogates (input signals) and tumor motion proposed by researchers are black box approaches [11], [12]. However, we felt that for relatively reliable long term prediction of tumor motion, a model which incorporates the knowledge of mechanical properties of the lung like tissue properties etc., is better suited.

The mechanical properties of lung tissues have been studied in detail by many researchers and the behavior has been characterized as viscoelastic and nonlinear [14], [15]. In the literature related to pulmonary mechanics, the dynamics of lung have often been described in terms of the pressure volume relationship [14] [16]. In these studies the pressure volume curves for the lung are also described to be hysteretic. Further, for small amplitude of deformation, major part of hysteretic behavior can be described by a linear viscoelastic model [14]. Traditionally, the study of mechanical properties of lung using methods such as pressure-volume relationships have been used for determining the physiological functions of the lung. These have been used to compare the properties of normal lung to the properties of a lung affected by diseases like Lung Fibrosis, Asthma, Emphysema, etc. [17]. In view of the extensive research already done

in representing the dynamical mechanical properties of lung tissue using pressure-volume model, we propose a hierarchical model for tumor motion comprising of two stages. In the first stage a fixed linear dynamical pressure-volume model is used to compute the output pressure from the tidal volume and then a nonlinear static mapping is used to find tumor position based on the output of the pressure-volume model (Figure 3).

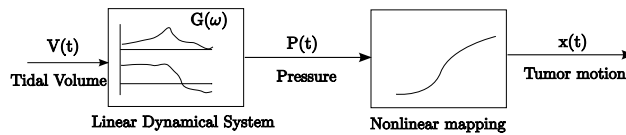


Fig. 3. Hierarchical scheme for modeling tumor motion

In the model presented above, the input is the tidal volume which is the volume of air a person is breathing in and out during normal respiration. This quantity can be measured at very high sampling rate (upto 1000 Hz) using spirometry measurements through an electronic pneumotachograph [18] [19]. In the experimental set-up used in this study we use a spirometer which measures the flow rate of the air being inhaled or exhaled and use numerical integration of flow-rate to find tidal volume.

1) *Linear Dynamic Model for Pressure-Volume Relationship:* An approach to derive the pressure-volume relationship for thin walled organs like lung in the form of a transfer function was described by Hilderbrandt [14]. One of the propositions of this work was that if the amplitude of deformation is relatively small (10-20% of operating volume), the hysteresis behavior is mainly of viscoelastic type which can be represented in linear form. Note that during normal human respiration, the tidal volume is about 500-600 ml which is around 10 % of the overall lung volume of around 6 Liters. For deriving the pressure-volume transfer function, a form of stress relaxation function (equation 1) was used to describe the pressure change in lung $p(t)$ as a transient response to step volume change of magnitude V_T .

$$\frac{p(t)}{V_T} = C - D \log t \quad (1)$$

Taking the laplace transform of this equation, we have

$$\frac{P(s)}{V_T} = \frac{C}{s} - \frac{D}{2.3s}(\Gamma'(1) - \ln(s)) \quad (2)$$

where $\Gamma'(1)$ is the derivative of Gamma function computed at 1 and is approximately equal to 0.5772. Now, for a step volume change of magnitude V_T , $V(s) = \frac{V_T}{s}$. Using this the Pressure-Volume transfer function can be written as

$$\frac{P(s)}{V(s)} = C - \frac{D}{2.3}(\Gamma'(1) - \ln(s)) \quad (3)$$

The transfer function derived from transient step response, equation 3, is then tested by comparing response of this model to actual response to sinusoidal inputs of varying frequencies. The author in [14] proposes that if the derived model can accurately represent response to the sinusoidal input as well as step input, then the model adequately represents material properties. It is shown in the same work that the frequency response calculated based on modeled transfer function closely represents the observed magnitude response to sinusoidal input, however the phase response for modeled frequency response function was persistently lagging the observed output by a third of the total phase.

Based on the model proposed in [14] we expand the natural log term in the transfer function approximated by a series expansion given by equation 4.

$$\ln(s) = 2 \left(\frac{s-1}{s+1} + \frac{1}{3} \left(\frac{s-1}{s+1} \right)^3 + \dots \right) \quad (4)$$

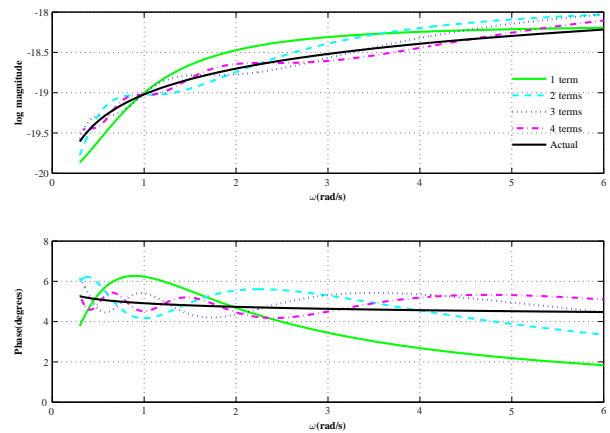


Fig. 4. Bode diagram of Pressure-Volume transfer function

Figure 4 shows the bode diagram of the approximated Pressure-Volume transfer function with increasing number of terms in the log expansion series. From this figure, it can be seen that in the frequency range of interest which ranges from 12-20 breaths per minute or 1.26 rad/s to 2 rad/s, that the series with the first three or four terms reasonably approximates the transfer function. Unknown parameters C and D , of the pressure-volume transfer function were obtained by minimizing the square of the error between the response of modeled transfer function and actual measurements using non linear least squares method for training data sets and with different number of terms in the log expansion series.

2) *Pressure-lung membrane displacement relationship:* As we are interested in the model for tumor motion, we now consider a model to represent the displacement of lung tissue corresponding to the change in pressure

during respiration. We use the relationships between pressure and displacement for lung tissue proposed by Ben-Haim et al. [20]. These are given by the equations:

$$P_{alv} - P_{pl} - \sigma_L = 0 \quad (5)$$

$$P_{gauge} = k_1 \sinh(k_3(\Delta X - k_2)). \quad (6)$$

In equation 5 P_{alv} is the alveolar pressure (pressure inside the lung) and P_{pl} is the pleural pressure, (pressure surrounding the lung). So the stress on the lung tissue σ_L is the difference of these two pressures. In our experimental setup the outside surface of lung tissue is exposed to atmosphere so σ_L is the gauge pressure inside the lung. In equation 6, the relationship between stress on lung tissue and the displacement is represented using a hyperbolic relation and k_1, k_2 and k_3 are parameters to be identified. Unknown coefficients for all the above relationship were identified by minimizing the square of the error between modeled and observed data for the training data set.

III. DATA COLLECTION

In order to study how respiration effects the motion of lung tumor an experimental setup consisting of porcine lung explant, air pump, VICON MX 3D motion capture system, flow and pressure sensors was constructed. To simulate how the lung tissue and objects attached to the tissue surface behave during respiration, an inflatable porcine lung explant (BioQuest Inflatable Lungs) [21] was used. The anatomical and physiological properties of porcine lungs are similar to human lungs and they have been used in variety of studies related to human lung [22]. The properties of porcine lungs used in this study were similar to that of a 65-70 Kilograms(140-160 lb.) human.

Tumors on the surface of the lung(parenchyma) are represented by attaching infra-red reflective markers. Motion of these markers is captured using Vicon MX motion capture system. Flow rate of the air flowing in and out of the lungs is measured using a differential pressure based flow sensor. A pressure sensor is also used to measure the pressure of air inside the lungs. For measuring the location of infra-red markers in realtime, the VICON MX motion capture sytem was utilized.

Marker position, pressure and flow rate data was collected using the test set-up for various scenarios. Infra-red markers were placed at multiple locations to analyze the effect of spatial variation on tumor motion. Breathing patterns mimicking real respiration were ensured while inflating and deflating the lung. To see the effect of respiration rate, scenarios for slow breathing and rapid breathing were also simulated. Figure III shows the tidal volume signal for the case of slow and rapid breathing.

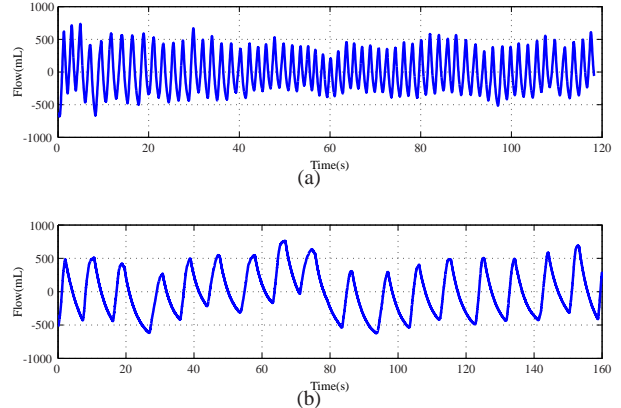


Fig. 5. Tidal volume signal for (a) rapid breathing, (b) slow breathing

IV. UNCERTAINTY QUANTIFICATION

The approach used for tumor motion modeling proposed in the previous section is a two stage procedure with a fixed pressure-volume model and patient and tumor position specific pressure-membrane displacement model. It was proposed that the fixed pressure-volume model can be developed using experimental procedures highlighted in Section 2 on large patient/lung explant data set. However, there can still be some variability in the model parameters across the large data set of patients which can also be characterized by experimental procedures as proposed in Section 2. Therefore, a study of modeling assumptions and their effect on the performance of the model is imperative for any reliable Image Guided Radiotherapy procedure based on the proposed framework. In this section, we focus on these modeling assumptions for the parameters associated with the Pressure-Volume model. We assume that these parameters are random variables. Based on the experimental data, first the problem of characterizing the distribution of these random variable is discussed. Next this knowledge is used to compute the uncertainty in model predictions using an efficient procedure based on stochastic Galerkin approach known as Polynomial Chaos. By quantifying the uncertainty in the model predictions using uncertainty measures like standard deviation, this framework can be used to make optimal decisions in real time about when to image the patient.

A. Distribution of Uncertain Model Parameters

In the original pressure-volume model the parameters C and D were considered as deterministic. In our new framework these parameters are considered as stochastic. However, the choice of probability distribution which represents these parameters is still an important consideration.

As the parameters learned from multiple data sets were found to be distributed over a particular range, we develop a Polynomial Chaos based framework with beta distribution as the probability model to represent random parameters C and D . The density function for beta distribution with support in the interval (a,b) is given as

$$p(x) = \frac{(x-a)^\beta(b-a)^\alpha}{(b-a)^{\alpha+\beta+1}B(\alpha+1,\beta+1)}, \quad a \leq x \leq b \quad (7)$$

where $B(p,q)$ is the beta function defined as

$$B(l,m) = \frac{\Gamma(l)\Gamma(m)}{\Gamma(l+m)} \quad (8)$$

and $\Gamma(\cdot)$ is the Euler gamma function. The beta distribution can be used to study a variety of distributions by varying the shape parameters α and β . Further the beta distribution becomes the uniform density when $\alpha = \beta = 0$. The shape parameters for the beta distribution can be evaluated from the observed experimental outcomes using a suitable statistical model. For numerical results we consider the uncertain parameters to be uniformly distributed ($\alpha = \beta = 0$) over the range between the maximum and minimum value of parameters learned for multiple data sets.

B. Polynomial Chaos

Polynomial Chaos(PC) is a representation of stochastic process as an infinite sum of Hermite orthogonal polynomials of Gaussian random variables (equation 9). This development was first introduced by Norbert Wiener [23] in 1938. Cameron and Martin [24] proved that for stochastic processes with finite second order moment this expansion converges in L^2 sense. PC expansion for a stochastic process $\mathbf{x}(t, \omega)$, where ω represents the uncertainty, is given by equation 9.

$$\mathbf{x}(t, \omega) = \sum_{i=0}^{\infty} \mathbf{x}_i(t) \Psi_i(\xi(\omega)) \quad (9)$$

Ghanem and Spanos [25] used this method to solve stochastic differential equations related to problems of solid mechanics by truncating the series sum to finite number of terms. They used the Galerkin projection approach on the truncated PC expansion, to obtain a set of *deterministic* differential equations corresponding to the coefficients of polynomial chaos expansion which can be solved numerically.

This procedure can be used for representing any stochastic process with finite second order moments. However, Xiu and Karniadakis [26] showed that the convergence of PC expansion using Hermite polynomials is exponential only for Gaussian process. They developed the generalized Polynomial Chaos(gPC) approach and showed

that exponential convergence can be reached for other types of random variables by using different orthogonal polynomials based on the distribution of uncertain parameters. This scheme is known as the Wiener-Askey scheme.

The main advantage in using this procedure is that we can potentially compute the uncertainty measures like standard deviations etc, associated with the stochastic process in real time and use that information in making decisions in real-time. In the pressure-volume model proposed in the previous section, there are maximum two uncertain parameters so the PC expansion approach is computationally more efficient than the Monte Carlo approach.

1) *General Procedure*: The general procedure for applying this procedure is demonstrated using the stochastic differential equation:

$$\dot{\mathbf{x}}(t, \mathbf{p}) = \mathbf{f}(t, \mathbf{u}(t); \mathbf{p}) \quad (10)$$

where, $\mathbf{x}(t, \mathbf{p})$ is the stochastic response of the system. $\mathbf{U}(t; \omega)$ is the input to the system. $\mathbf{p} \in \mathbb{R}^m$ is a vector of uncertain parameters, which are functions of random variable $\xi \in \mathbb{R}^m$ with known pdf $f(\xi)$. The stochastic state and uncertain parameters can be represented by finite PCE

$$\mathbf{x}(t, \xi) \approx \sum_{i=0}^N \mathbf{x}_i(t) \Psi_i(\xi) \quad (11)$$

$$\mathbf{p}(\xi) = \sum_{i=0}^N \mathbf{p}_i \Psi_i(\xi) \quad (12)$$

where $\mathbf{x}_i(t)$ are the deterministic polynomial chaos coefficients, $\Psi_i(\xi)$ are the multidimensional orthogonal polynomials of random variables ξ with highest order p . The dimension of vector of random variables $\xi(\omega)$, m , is the same as the number of uncertain parameters in the system. Multidimensional orthogonal polynomials are generated using the tensor product of one dimensional orthogonal polynomials, thus the total number of terms in equation 12 ($N+1$) are given by:

$$N + 1 = \frac{(p+m)!}{p!m!} \quad (13)$$

Error due to finite PCE is given as

$$\mathbf{e}(\xi) = \sum_{i=0}^N \dot{\mathbf{x}}_i(t) \Psi_i(\xi) - \mathbf{f}(t, \mathbf{u}(t); \sum_{i=0}^N \mathbf{p}_i \Psi_i(\xi)) \quad (14)$$

Now, this error is minimum if the Galerkin projection of the above equation on to each of the orthogonal polynomial $\Psi_k(\xi)$ is zero.

$$\langle \mathbf{e}(\xi), \Psi_i(\xi) \rangle = 0$$

where $\langle \cdot, \cdot \rangle$ represents the ensemble average or the inner product operator. This leads to a set of deterministic differential equations which can be solved numerically for the PCE coefficients.

C. Polynomial Chaos Formulation For Proposed Model

In this section the PCE is applied to the prediction models proposed in Section 2. As discussed in section IV-A, the uncertainty measures for the model are computed assuming the parameters are random variables with beta distribution.

The pressure volume transfer function model of lung in Section 3 with three terms in log expansion series can be written as

$$\frac{P}{V}(s) = c - \frac{d}{2.3}(\Gamma'(1) - \ln(s)) \quad (15)$$

$$\approx \frac{(c + 1.4d)s^3 + (3c + .8d)s^2 + (3c + .8d)s + (c - .9d)}{s^3 + 3s^2 + 3s + 1}$$

where c and d are independent random variables with beta distribution given by

$$d = \text{Beta}(\alpha_d, \beta_d); d_l \leq d \leq d_u; c = \text{Beta}(\alpha_c, \beta_c); c_l \leq c \leq c_u.$$

Writing the above transfer function in state space observable canonical form we have,

$$\dot{\mathbf{x}}(t) = \underbrace{\begin{bmatrix} -3 & 1 & 0 \\ -3 & 0 & 1 \\ -1 & 0 & 0 \end{bmatrix}}_{\mathbf{A}} \mathbf{x}(t) + \underbrace{\begin{bmatrix} -3.48 \\ -3.48 \\ -2.32 \end{bmatrix}}_{\mathbf{B}} d \times V(t) \quad (16)$$

and the output equation is

$$P(t) = \underbrace{\begin{bmatrix} 1 & 0 & 0 \end{bmatrix}}_{\mathbf{C}} \mathbf{x}(t) + \underbrace{(c + 1.41d)}_{\mathbf{D}} V(t) \quad (17)$$

According to the Wiener-Askey polynomial chaos scheme, for exponential convergence of polynomial chaos for Beta distribution the expansion should be written in terms of Jacobi orthogonal polynomials. As only parameter d appears in the state space equation 16, we will represent the stochastic state variable \mathbf{x} in terms of 1-D polynomial chaos. The expansion for random variable, d , using Jacobi polynomials $\Psi_k(\xi)$ is:

$$d = d_0\Psi_0(\xi) + d_1\Psi_1(\xi) + 0 + \dots + 0 \quad (18)$$

where ξ is a beta distributed random variable given by the equation

$$\xi = \text{Beta}(\alpha_d, \beta_d); -1 \leq \xi \leq 1$$

d_0 is $E[d]$ i.e. expected value of parameter d and d_1 can be calculated using the equation

$$d_1 = \frac{\langle d, \Psi_1(\xi) \rangle}{\langle \Psi_1(\xi), \Psi_1(\xi) \rangle}$$

As the stochastic state variable $\mathbf{x}(t)$ depends only on the random variable d , the PC expansion of the state can be

written in terms of one dimensional polynomial chaos as

$$\mathbf{x}(t) = \sum_{i=0}^{i=N} \mathbf{x}_i(t)\Psi_i(\xi) \quad (19)$$

Using these expansions in equation 16 we get,

$$\sum_{i=0}^N \dot{\mathbf{x}}_i(t) = \mathbf{A} \sum_{i=0}^N \mathbf{x}_i(t)\Psi_i(\xi) + \mathbf{B} \sum_{i=0}^N d_i\Psi_i(\xi)V(t) \quad (20)$$

Galerkin projection of equation 20 onto the space spanned by orthogonal polynomials $\Psi_k(\xi)$ leads to k^{th} constraint equation

$$\dot{\mathbf{x}}_k(t) = \frac{\mathbf{A}\mathbf{x}_k(t)\langle \Psi_k(\xi), \Psi_k(\xi) \rangle + \mathbf{B}d_k\langle \Psi_k(\xi), \Psi_k(\xi) \rangle V(t)}{\langle \Psi_k(\xi), \Psi_k(\xi) \rangle} \quad (21)$$

This leads to a set of $3(N+1)$ deterministic differential equations given by

$$\dot{\mathcal{X}} = \mathcal{A}\mathcal{X} + \mathcal{B}V(t) \quad (22)$$

These deterministic equations can be solved for the coefficients of the stochastic state variable for time varying input $V(t)$. Then using the output equation 17 we can find the mean of predicted pressure as

$$\begin{aligned} \mu_P &= E[P(t)] = E\left[\sum_{i=0}^N x_i^{(1)}(t)\Psi_i\xi + (c + 1.41d)V(t)\right] \\ &= x_0^{(1)}(t) + (\mu_c + 1.41\mu_d)V(t) \end{aligned} \quad (23)$$

and variance $\sigma_P^2(t) = \text{Var}[P(t)]$ can be computed as

$$\begin{aligned} \sigma_P^2(t) &= E\left[\left(\sum_{i=0}^N x_i^{(1)}(t)\Psi_i\xi + (c + 1.41d)V(t)\right)^2\right] - \mu_P^2 \\ &= \sum_{i=0}^N \left(x_i^{(1)}(t)\right)^2 E[\Psi_i^2(\xi)] + (\mu_c^2 + \sigma_c^2 + 1.41^2(\mu_d^2 + \sigma_d^2)) V(t)^2 \\ &\quad + 2 \times 1.41 \left(\sum_{i=0}^N x_i^{(1)} d_i E[\Psi_i^2(\xi)]\right) V(t) - \mu_P^2(t) \end{aligned} \quad (24)$$

The inner product for Jacobi polynomials can be calculated using the following relation [26]

$$\begin{aligned} E[\Psi_i^2(\xi)] &= \int_{-1}^1 \Psi_i^2(\xi)p(\xi)d\xi \\ &= \frac{\Gamma(i+\alpha+1)\Gamma(i+\beta+1)}{(2i+\alpha+\beta+1)B(\alpha+1,\beta+1)\Gamma(i+\alpha+\beta+1)i!} \end{aligned} \quad (25)$$

where $B(\alpha + 1, \beta + 1)$ is the beta function.

1) *Numerical Results:* The procedure described in the previous section was used to generate numerical results for the pressure-volume model. In this section results for the case when both parameters of the model are considered as random with uniform distribution are presented. Shape and location parameters of the beta distribution for the two random variables are given in table I

Figure 6 shows the evolution of mean(red-dashed) and

TABLE I
SHAPE AND LOCATION PARAMETERS FOR BETA DISTRIBUTION

	c	d
α	0	0
β	0	0
a	.0175	.0027
b	.024	.0113

$\pm 3\sigma$ bounds of predicted pressure time upto 20 seconds. The actual measured pressure(blue-dotted) is also shown in the figure. We can see that the variance is highest at the peaks and thus new information from the imaging system can be collected at these times for accurate tracking of tumor location. We also see from the figure that the measured pressure lies within the predicted $\pm 3\sigma$ bounds for most of the time.

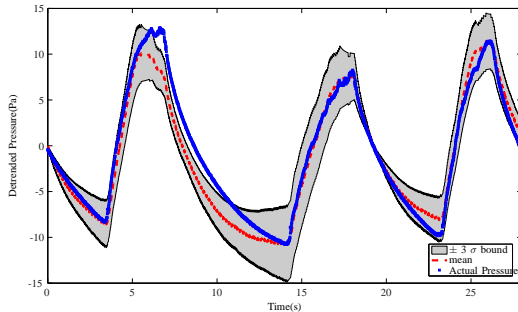


Fig. 6. Mean and 3σ bounds for detrended pressure

Comparison of pdfs and histograms for the polynomial chaos expansion of fourth order and Monte Carlo simulation with 10,000 samples is shown in figure 7. As can be seen from these figures PC expansion approximates the pdfs well at all time steps. Evolution of pdfs using PC expansion for predicted pressure is shown in figure 8. Relatively higher variance at peaks in pressure value is also apparent from this figure.

V. CONCLUSIONS

This paper addresses the issue of estimation of uncertainties associated with estimated states of tumors motion. A classic pressure-volume dynamic model in conjunction with a previously presented pressure-displacement algebraic model is proposed to be used. Probability density functions of the model parameters are used to express the stochastic states using a polynomial chaos series expansion. Numerical simulations are used to illustrate the accurate reproduction of the distribution of the model states as a function of time. Monte Carlo simulations are used to create the reference distribution for comparison.

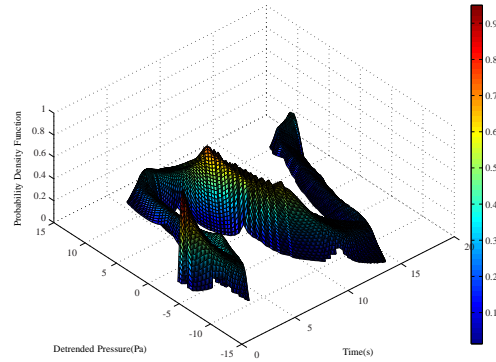


Fig. 8. Evolution of pdf of predicted detrended pressure using polynomial chaos

VI. ACKNOWLEDGEMENT

This work was supported by NSF Award No. CMMI-0928630

REFERENCES

- [1] A. M. Allen, K. M. Siracuse, J. a. Hayman, and J. M. Balter, "Evaluation of the influence of breathing on the movement and modeling of lung tumors.," *International journal of radiation oncology, biology, physics*, vol. 58, pp. 1251–7, March 2004.
- [2] Y. Seppenwoolde, H. Shirato, K. Kitamura, S. Shimizu, M. V. Herk, J. V. Lebesque, and K. Miyasaka., "Precise and real-time measurement of 3d tumor motion in lung due to breathing and heartbeat, measured during radiotherapy.," *Radiation Oncology*, vol. 53, pp. 822– 834, 2002.
- [3] L. P. Muren, G. Maurstad, R. Hafslund, G. Anker, and O. Dahl, "Cardiac and pulmonary doses and complication probabilities in standard and conformal tangential irradiation in conservative management of breast cancer.," *Radiotherapy and oncology : journal of the European Society for Therapeutic Radiology and Oncology*, vol. 62, pp. 173–83, February 2002.
- [4] E. SENKUSKONEFKA and J. JASSEM, "Complications of breast-cancer radiotherapy.," *Clinical Oncology*, vol. 18, pp. 229–235, April 2006.
- [5] P. Mavroidis, S. Axelsson, S. Hyödynmaa, J. Rajala, M. A. Pitkänen, B. K. Lind, and A. Brahme, "Effects of positioning uncertainty and breathing on dose delivery and radiation pneumonitis prediction in breast cancer.," *Acta Oncologica*, vol. 41, pp. 471–485, September 2002.
- [6] L. A. Dawson and D. A. Jaffray, "Advances in image-guided radiation therapy.," *Journal of clinical oncology : official journal of the American Society of Clinical Oncology*, vol. 25, pp. 938–46, March 2007.
- [7] M. J. Murphy, "Tracking moving organs in real time.," *Seminars in radiation oncology*, vol. 14, pp. 91–100, January 2004.
- [8] H. Shirato, S. Shimizu, K. Kitamura, T. Nishioka, K. Kagei, S. Hashimoto, H. Aoyama, T. Kunieda, N. Shinohara, H. Dosaka-Akita, and K. Miyasaka, "Four-dimensional treatment planning and fluoroscopic real-time tumor tracking radiotherapy for moving tumor.," *International journal of radiation oncology, biology, physics*, vol. 48, pp. 435–42, September 2000.
- [9] D. Ruan, J. A. Fessler, and J. M. Balter, "Mean position tracking of respiratory motion.," *Medical Physics*, pp. 782–792, 2008.
- [10] P. Singla, T. Singh, and A. Schweikard, "A multiresolution adaptive approach for respiratory motion modeling.," *2007 IEEE/NIH Life Science Systems and Applications Workshop*, pp. 23–26, November 2007.
- [11] H. Wu, G. C. Sharp, B. Salzberg, D. Kaeli, H. Shirato, and S. B. Jiang, "A finite state model for respiratory motion analysis in image guided radiation therapy.," *Physics in Medicine and Biology*, vol. 49, pp. 5357–5372, December 2004.

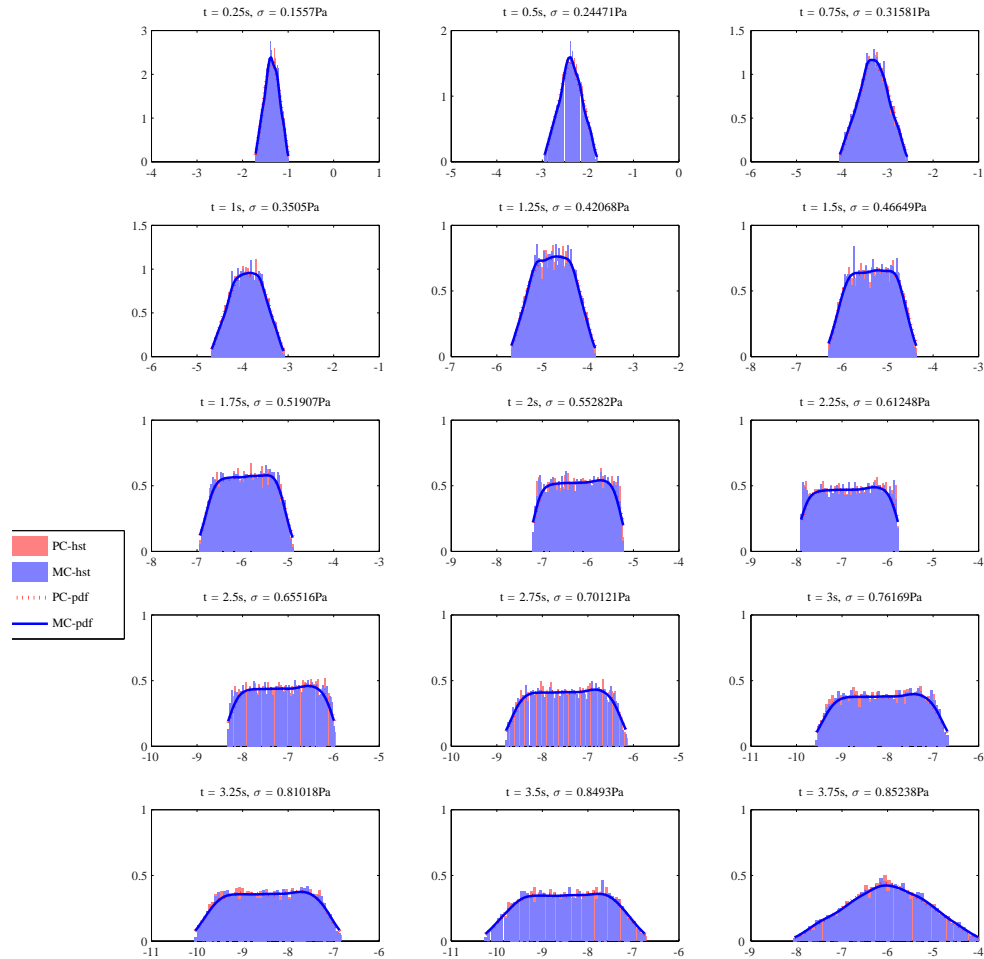


Fig. 7. Pdf of predicted detrended pressure at every 0.25 seconds from .25s to 3.75 s.

- [12] D. A. Low, P. J. Parikh, W. Lu, J. F. Dempsey, S. H. Wahab, J. P. Hubenschmidt, M. M. Nystrom, M. Handoko, and J. D. Bradley, "Novel breathing motion model for radiotherapy," *Int. J. Radiation Oncology Biol. Phys.*, vol. 63, pp. 921–929, 2005.
- [13] D. Ruan, J. A. Fessler, and J. M. Balter, "Real-time prediction of respiratory motion based on local regression methods.," *Physics in medicine and biology*, vol. 52, pp. 7137–52, 2007.
- [14] J. Hilderbrandt, "Comparison of mathematical models for cat lung and viscoelastic balloon derived by laplace transform methods from pressure-volume data.," *Bulletin of Mathematical Biology*, vol. 31, pp. 651–667, 1969.
- [15] H. Yuan, S. Kononov, F. S. Cavalcante, K. R. Lutchen, E. P. Ingenito, and B. Suki, "Effects of collagenase and elastase on the mechanical properties of lung tissue strips.," *Journal of applied physiology (Bethesda, Md. : 1985)*, vol. 89, pp. 3–14, July 2000.
- [16] W. Tomalak, R. Peslin, and C. Duvivier, "Respiratory tissue properties derived from low transfer function in healthy humans," *Journal of Applied Physiology*, vol. 82, pp. 1098–1106, 1997.
- [17] D. S. Faffe and W. a. Zin, "Lung parenchymal mechanics in health and disease.," *Physiological reviews*, vol. 89, pp. 759–75, July 2009.
- [18] H. D. Kubo and B. C. Hill, "Respiration gated radiotherapy treatment: a technical study.," *Physics in medicine and biology*, vol. 41, pp. 83–91, January 1996.
- [19] J. D. P. Hoisak, K. E. Sixel, R. Tirona, P. C. F. Cheung, and J.-P. Pignol, "Correlation of lung tumor motion with external surrogate indicators of respiration.," *International journal of radiation oncology, biology, physics*, vol. 60, pp. 1298–306, November 2004.
- [20] S. A. Ben-Haim, O. Lichtenstein, and G. Saidel M., "Mechanical analysis of extrapulmonary volume displacements in the thorax and abdomen," *Journal of Applied Physiology*, vol. di, 1989.
- [21] ENasco, "Bioquest inflatable lungs kit."
- [22] C. S. Rogers, W. M. Abraham, K. a. Brogden, J. F. Engelhardt, J. T. Fisher, P. B. McCray, G. McLennan, D. K. Meyerholz, E. Namati, L. S. Ostedgaard, R. S. Prather, J. R. Sabater, D. A. Stoltz, J. Zabner, and M. J. Welsh, "The porcine lung as a potential model for cystic fibrosis.," *American journal of physiology. Lung cellular and molecular physiology*, vol. 295, pp. L240–63, August 2008.
- [23] N. Wiener, "The homogeneous chaos," *American Journal of Mathematics*, vol. 60, pp. 897–936, 1938.
- [24] R. Cameron and W. T. Martin, "The orthogonal development of non-linear functionals in series of fourier-hermite functionals," *Annals of Mathematics*, vol. 48, pp. 385–392, 1947.
- [25] R. G. Ghanem and P. D. Spanos, *STOCHASTIC FINITE ELEMENTS: A Spectral Approach*. Springer-Verlag, 1991.
- [26] D. Xiu and G. E. Karniadakis, "The wiener-askay polynomial chaos for stochastic differential equations," *SIAM Journal on Scientific Computing*, vol. 24, p. 619, 2002.